Proceedings of ASME Turbo Expo 2025
Turbomachinery Technical Conference and Exposition
GT2025
June 16-20, 2025, Memphis, Tennessee

GT2025-152113

Research on the Flow Field and Performance Characteristics of a Novel Reference Design Centrifugal Compressor for Refrigerant Compression

Vlad Goldenberg
SoftInWay, Inc
Burlington, MA

Ben Conser
SoftInWay, Inc
Burlington, MA

Andrey Sherbina
SoftInWay Switzerland GmbH
Zug, Switzerland

Anna Vorobyova
SoftInWay Switzerland GmbH
Zug, Switzerland

ABSTRACT

Compression of heavy hydrocarbons and refrigerants is an important task for a large collection of centrifugal compressors in various industrial applications. However, most applied research on the optimum design and flow field of centrifugal compressors relied on data gathered based on air as a working fluid. While it is recognized that dimensionless correction for gas dynamic parameters enables a broad understanding of the fundamental fluid dynamics, there are nevertheless unique attributes of machine design that are optimum specifically for heavy hydrocarbon and refrigerant type fluids. This work specifically addresses this gap.

More specifically, a set of reference designs was developed for a compressor using R134a as the working fluid with boundary conditions corresponding to a typical heat pump application. The design uses an integrally shrouded impeller wheel, which is often employed in process and refrigeration compression systems. The design set we show is suited to scaling for variations in flow rate capacity and can also be employed in a multistage design. Furthermore, several variants of the design are available as baselines depending on whether peak efficiency or high surge margin is sought, depending on the desired performance.

This paper describes the design strategy of a refrigeration (R134a) centrifugal compressor for achieving the best value of the surge margin and increasing the operational range of the compressor. The initial design of the centrifugal compressor was developed in 2D code and analyzed using 1D and 2D methodologies. Analytical results show good agreement between 2D code and 3D CFD analysis using Ansys CFX at the design point for an initial design but may not satisfy off-design operational requirements for a broad range of applications. The focus of the research is to develop a centrifugal compressor with improved surge margin. The current work includes the analysis of several compressor designs and the comparison of operational maps between each other and links the important design and fluid dynamic variables across the operating range to characteristics of the compressor. Impeller geometry modifications, such as blade angle distribution, in conjunction with rotating speed variability, which have a major influence on the aerodynamic parameters of compressors, can reduce blade aerodynamics loads and increase the operational range of a compressor. Additionally, the work is focused on analyzing the influence of loss models on performance maps. 1D analyses and profiling methodologies are implemented using 2D code. The meridional geometry of the impeller, vaneless diffuser, and volute are maintained through the design variations such that components can be substituted in application. Additionally, boundary conditions at the compressor inlet are fixed. All compressor designs have unique attributes that contribute to, or may be attributable to, specific characteristics of their performance. Verification of the performance map and surge margin was carried out using the commercial CFD code Ansys CFX and compared with results from 1D/2D analysis and tuned to well-known models. This results in a 10% increase in mass flow rate-based surge margin. Results from the research can be used for the development of refrigeration compression systems as single-stage or multistage compressors designs.

Keywords: centrifugal compressor, refrigerant R134a, surge; surge margin, performance map.

NOMENCLATURE

dβ/dm	derivative of blade angle by meridian length at outlet
Pt inlet	total pressure at inlet
Tt inlet	total temperature at inlet
n	rotational speed
ps_out	static pressure at outlet
SM	surge margin
PR_w	pressure ratio in the design point
PR_s	pressure ratio in the stall/surge point
$\dot{m}$	mass flow rate

σ_s	slope factor
Cu	tangential component of the absolute velocity at blade outlet (index 2) and at blade outlet in ideal conditions (2∞)

1. INTRODUCTION

Modern compressor design targets require high performance and a wide operating range to increase the operational usefulness of the machine. It is recognized that a large collection of literature exists on general design methodologies of centrifugal compressors, and that there are even a few notable open literature cases that are available for workers in this field to use as reference and validation cases. These open cases include that of Krain [1], Radiver [2, 3], and HECC [4]. Notably, all open research cases are based on air (appropriately) and are characteristic of aerospace application machines. Centrifugal compressors designed for air and refrigerant compressors differ in the fluid properties they handle, the operating conditions, and the design considerations involved. Refrigerant compressors typically require more sophisticated designs to handle high-pressure ratios, phase changes, and temperature variations. In contrast, air compressors have simpler designs and focus on handling low-density gases under stable conditions. When comparing these designs, key areas to focus on include impeller geometry, volute and diffuser design, efficiency, and surge margin. Understanding these differences is essential when selecting or designing a compressor for a specific application. Notably, all open research cases are based on air (appropriately) and are characteristic of aerospace application machines. Thus, we saw a paucity of good references for open-access process style machines and especially heavy hydrocarbon/fluorocarbon machines that operate on fluids close to the vapor region and whose fluid is poorly represented by the ideal gas model. The aim and objectives of the current work includes the development of a good “reference” compressor for an R134a application typical of a refrigeration cycle or heat pump.

In this scope of research, the analysis of several compressor designs, comparison of operating maps, investigation of loss model influence on performance maps, and improvement of the surge/stall margin of compressor designs will be explored. It is recognized that certain application operational ranges are dictated in different ways. For example, surge margin is more sensitive for heat pump applications because the 1st order dynamics of the thermal boundary conditions directly impact the outlet pressure requirement of the compressor, and the flow is only a 2nd order and higher effect.

Centrifugal compressors play a significant role in refrigeration as they efficiently compress the refrigerant, which is a key component of the thermal management system. However, traditional compressor designs face challenges such as reduced efficiency and operating range under different operating conditions. Another key point is that compressor designs often have limited surge margin, which leads to instability and reduced system reliability. Surge margin is a critical performance parameter as it determines the compressor's ability to avoid surges and maintain stable operation. Surges can cause pressure fluctuations and compressor instability, which can negatively impact the efficiency and lifespan of the entire system. An overview of different locations where these effects can occur in a radial machine is given by Liskiewicz [6]. The inflow condition can be already disturbed before the flow enters the impeller, which was estimated by Katz [7]. Surge is an unstable flow phenomenon characterized by the interruption of fluid flow in the entire compression system consisting of the compressor, its inlet and outlet piping, downstream throttling devices, etc. [8]. Surge is always accompanied by a sudden drop in pressure rise, and stall occurs close to the peak of the total-static pressure rise characteristic [9]. Once stall is fully developed, the circumferentially averaged mass flow and pressure ratio remain almost constant. These features provide the basis for judging surge, as well as simulating the occurrence of surge [10, 11].

In response to these challenges, the development of a novel reference design for centrifugal compressors has attracted significant attention. The objective of this study is to investigate the flow field and performance characteristics of such a design, focusing on optimizing the compressor's aerodynamic performance and increasing its surge margin while considering factors such as refrigerant type, operating speed, and geometry modification. A novel reference design of a centrifugal compressor to meet these challenges and the development of new reference designs for centrifugal compressors has attracted significant attention. The objective of this study is to investigate the flow field and performance characteristics of such designs, focusing on optimizing the compressor's aerodynamic performance and enhancing the surge limit, considering factors such as refrigerant type, operating speed, and geometry changes. The new reference design for centrifugal compressor includes an impeller, a vaneless diffuser, and a volute.

The compressor in this study assumes the general principles of centrifugal compression but introduces flexibility in certain design elements to meet different operating objectives. In particular, the compressor volute shape and overall meridian profile remain constant, but parameters related to the impeller geometry such as the blade outlet metal angle, the number of blades, and changes in the beta/theta distribution (i.e., the blade angle along the span of the impeller) are variable. This study provides a systematic approach to understanding the relation between impeller design and compressor performance. The results will help develop centrifugal compressor candidates that can be applied in specific heating, ventilation, and air conditioning (HVAC) industries.

All compressor design candidates are analyzed using 1D/2D analysis methods in 2D code, a turbomachinery design, simulation and optimization tool. Using 2D code for 1D/2D analysis allows the researchers to efficiently evaluate and compare different impeller geometries while maintaining consistency for other components of the compressor. This approach provides a detailed understanding of how impeller design affects compressor performance and helps determine the optimal configuration for different HVAC applications.

Furthermore, by incorporating advanced computational fluid dynamics (CFD) simulations, this study aims to provide insight into potential improvements in compressor efficiency and performance. Recent studies have highlighted the importance of understanding the complex fluid dynamics of centrifugal compressors and the interaction between compressor components and refrigerant flow [12][13].

The calibration process of the loss models in 2D code based on 3D CFD results is an approach to improve the accuracy of the 1D centrifugal compressor performance predictions. Combining these tools allows for better prediction of compressor performance, which is critical in developing more efficient and reliable design for refrigerant applications. The main goals of this research are:

- Modifying the impeller geometry, especially the blade metal angle and number of blades, in order to increase the surge limit.
- Describing the affect the internal flow field affects. This study uses CFD simulations to investigate the impact of impeller geometry on flow distribution and performance characteristics.
- Implementing the calibration process of the loss models in 2D code based on 3D CFD result for better prediction of compressor performance.

2. MATERIALS AND METHODS

2.1 General 1D/2D 2D code Methods

All compressor designs in this study are created using 1D analysis methods with AxSTREAM™[14, 15], a software for turbomachinery design and optimization. Integrated 2D code provides a meanline/streamline method for generating and analyzing compressor geometries and performance predictions. The 1D analysis allows for fast and effective evaluation of unique design modifications, making it an ideal tool for early-stage design development. The main features of 2D code that are used in this study are:

- performance prediction: 2D code can predict the compressor efficiency, pressure rise, and other kinematics and thermodynamics parameters based on the selected design settings and boundary conditions. This gives ability to assess the impact of changing impeller geometry on overall performance;
- geometric optimization: The software supports the creation and modification of impeller geometries, allowing for detailed simulation of how different blade angles, number of blades, and other design parameters influence compressor behavior.

2.2 General CFD Methods

In this paper, computational fluid dynamics (CFD) was used as the main analytical method of validation analysis. This allows for the investigation of difficult structures in a fully three-dimensional flow and contains the fundamental physical equations such as mass, momentum, and energy conservation. CFD uses first-principles physics and semi-empirical models (turbulence and RANS) to solve for fluid thermodynamic (pressure, etc.) and kinematic (velocity vector) fields. These fields represent physical quantities.

In this work, a steady-state approach and viscosity terms were used for extracting the overall compressor characteristics. The turbulent viscosity was solved using the k-Epsilon turbulence model, which has wide applicability to common industrial flows.

A moving reference frame (MRF) model was used for blade motion modeling in steady-state analysis. A mixing plane interface was applied for connecting the interfaces between moving and stationary domains. Total pressure and total temperature were used as inlet boundary conditions. Static pressure was used as outlet boundary conditions. The hub and shroud surfaces were set as walls (rotating and stationary surfaces) and a periodic interface was used to model and define a cyclic/repeating situation of the flow across the boundary surface. The 3D view is shown in Figure 1.

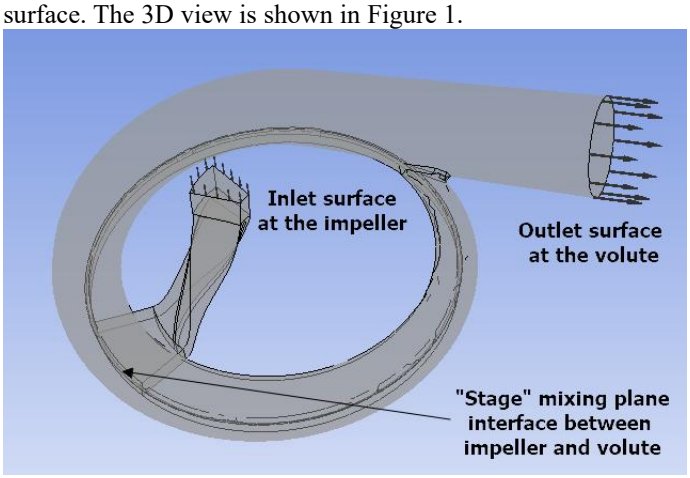

Figure 1: Computational domain for the 4-stage radial blower

For all compressor designs, the working fluid was set as real gas properties tables for refrigerant R134a which are generated using NIST RefPROP [13].

While R134a continues to be a widely used refrigerant, its high Global Warming Potential and energy inefficiencies are significant drawbacks in the context of global efforts to reduce greenhouse gas emissions. Newer refrigerants like R1234yf, R452B, and R1233zd provide lower Global Warming Potential, environmentally friendly alternatives with various performance benefits. However, each of these newer refrigerants also presents challenges, including flammability, cost, and compatibility with existing systems [16], [17]. Considering these statements, R134a was selected as the working fluid for the development of flexible, adaptable centrifugal compressors tailored for specific Heating, Ventilation, and Air Conditioning (HVAC) applications.

There were some initial difficulties in modeling the fluid properties in CFX, especially near the inlet, because the inlet boundary conditions are situated near the saturation line and two-phase region. Modeling real gases in CFD near the saturation line

or during phase transitions (liquid-vapor equilibrium) can be incredibly challenging due to several reasons:

- real gases exhibit non-ideal behavior, especially near the saturation line where both liquid and vapor phases coexist. The ideal gas law does not apply here, and thermodynamic properties (like pressure, temperature, and volume) can change non-linearly.

- the properties of the fluid (e.g., density, enthalpy, and entropy) change dramatically near the saturation line. Near the phase transition, sharp gradients or discontinuities can develop, which are hard to capture numerically and lead to solution convergence instability.

- numerical instability can occur when properties of the fluid are vastly different across the phases and near saturation line. Discontinuities in velocity, pressure, and temperature are common at the phase boundary, and handling these with numerical schemes is difficult.

When inlet properties from 2D code and CFX were compared to those from REFPROP, it was found that there were negligible differences in enthalpy and entropy (lower than 1%). This sort of discrepancy is acceptable.

2.3 Subject Cases and Mesh Settings

In this paper, three compressor designs were used for the research of the flow field and performance characteristics for refrigerant compression. The compressor design contains an impeller, vaneless diffuser, and volute. The geometries of the compressor designs were exported from 2D code to Ansys tools. Meshes for each of the impeller designs were computed in Ansys Turbogrid (Figure 5) and a volute mesh was created in Ansys Workbench mesh tool (Figure 6). The mesh was split in Ansys Turbogrid in order to model both the impeller and vaneless diffuser space. It is important to note that the geometry and mesh were the same for the volutes in the Ansys Workbench mesh tool.

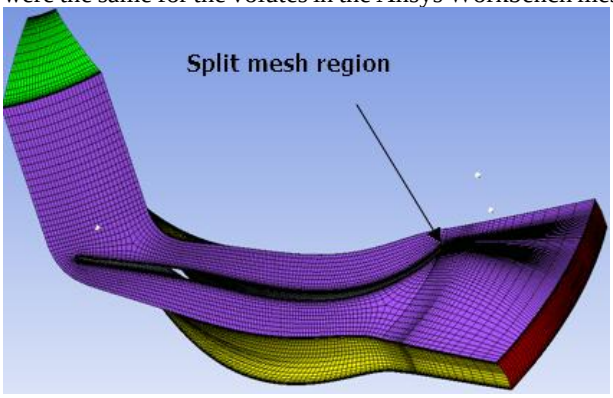

Figure 5: Example of mesh for the impeller in Ansys Turbogrid

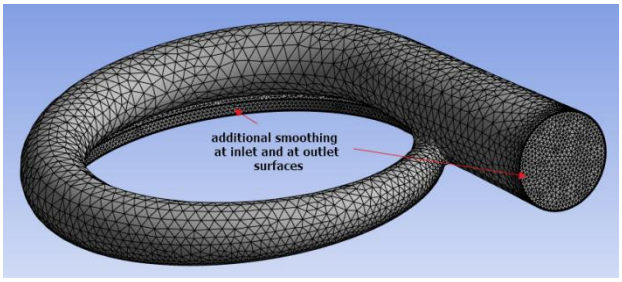

Figure 6: Example of mesh for the volute in Ansys Workbench mesh tool

Statistics for the mesh cells number for the computational domains are presented in Table 1.

Table 1. Mesh statistics

Domain	Number of mesh cells
Impeller. Original design	221424
Impeller. Design 2	286784
Impeller. Design 3	295710
Volute	182750

The impeller moving domain and volute stationary domain were used for the CFD analysis. A mixing plane “Stage” interface with a pressure averaging method was selected as the interface between the moving and stationary domains. The moving domain contains the impeller part with blade and the vaneless diffuser part. The hub and shroud of the vaneless diffuser have a counter rotating option, which means these surfaces were stationary even though they are in the moving impeller domain.

The K-Epsilon turbulence model was used with a turbulence intensity of 1% (Low). A Y+ analysis showed the advisability of the selected turbulence models (Figure 7).

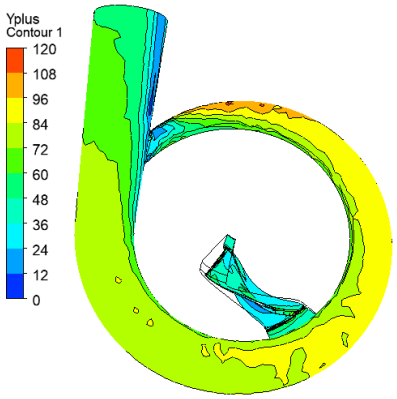

Figure 7: Example of Y+ distribution in compressor CFD domains

Boundary conditions for the CFD simulations are described in Table 2.

Table 2. Boundary conditions for CFD analysis

Boundary conditions	Units	Original design	Design 2	Design 3
Pt inlet	kPa	435		
Tt inlet	K	301.3		
n	RPM	63000	65800	66800
ps_out	kPa	range of pressure for operating map		
Turbulence model	-	k-Epsilon		
Turbulence intensity	%	1 (Low)		
Fluid	-	real gas properties tables refrigerant R134a		

2.3 Stall/Surge analysis

Except for the goal of developing a compressor characteristic across an operating range, the main point of research is to characterize the surge margin and increase it by expanding the operational compressor range. There are several useful parameters generated in the solution of most commercial CFD solvers. Here they are characterized into three classes:

• Residual metrics – numerical stability.

It is common to characterize solution numerical convergence as a root-mean-square (RMS) or maximum value of the equation residuals for each element, and for each specific equation.

• Physical imbalances.

These parameters indicate the physical soundness of the solution regarding preserving the physical conservation laws (mass, momentum, energy) for the domains or regions of the simulation. Some solvers (Ansys CFX, for example) include such parameters as default metrics to use for convergence evaluation and other uses. Others may require users to write functions dependent on field variables. These should have a relative value below 0.01 at a minimum, with typical values being much less to consider a particular iteration to be valid.

• Physical parameters – derived from field functions.

These are the resulting parameters, such as the mass flow rate at a boundary, the mass flow averaged total enthalpy, the isentropic efficiency, or multitudes of other parameters of interest [17].

There are many uncertainties concerned with stall and surge: uncertainties of prediction for a given design and uncertainties associated with the conditions of operation. Aerodynamic instability is one of the key concerns in compressor design, and rotating stall and surge are two typical instability phenomena. The former is characterized by high frequency and small-amplitude circumferential pressure pulsations, which cause the reduction of isentropic efficiency and blade fatigue. In contrast, the latter is characterized by the reversal of flow in the mainstream, which results in rapid performance degradation and even engine shutdown. What is worse, the reversal of flow during surge can cause structural damage. The profound consequences of aerodynamic instability mean it is always a key point in academic research and engineering practice [18].

There are many ways of defining surge margin, but one of the simplest methods can be defined by:

$$SM = (PR_S - PR_W)/PR_W \quad (1)$$

Where PR_W is the pressure ratio on the working line for a given corrected rotational speed and PR_S is the pressure ratio at the surge point on the same speedline (Figure 8).

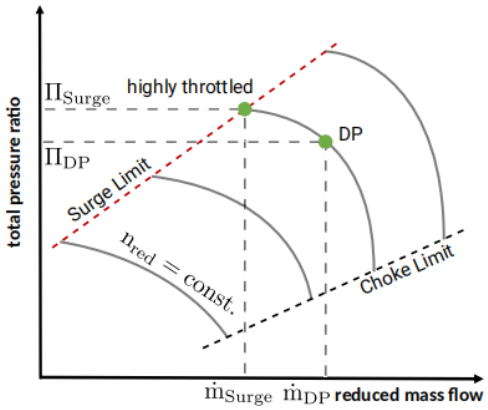

Figure 8: Surge margin definition via pressure slope [ijtpp-04-00042-v2]

A more general method of the surge margin definition is [20]:

$$\text{Surge margin} = 1 - \left\{\frac{PR_W}{PR_S} \times \frac{\dot{m}_S}{\dot{m}_W}\right\} \quad (2)$$

3. RESULTS AND DISCUSSION

One of the main target goals of redesigning the compressor was increasing the surge margin of the compressor performance maps. The main concept of research work for modifications of design geometry models was impeller geometry modification in in order to reduce the blade aerodynamics loads and increasing the operational range of the compressor. The volute and overall meridional profile of the compressor were held constant in order to more easily compare how different impeller design affects compressor performance. The main idea of constant compressor overall dimensions was to develop an optimal design with increased surge margin, fundamentally influence the operational characteristics of the machine, and apply it into an existing system of HVAC industries. The blade outlet metal angle, number of blades, and blade angle distributions were changed during the research. Besides aerodynamic influences, the impeller geometry affects the secondary flow and parasitic work

in the impeller. A high number of blades means an almost blade-compliant flow guidance leading to a small reduction in deflection [20]. If the blade curves backwards, the flow separation on the blade suction side decreases, since the relative flow is decelerated over a longer distance with the same pressure ratio [21, 22].

Design points for all compressors (Figure 9) were the same as the required mass flow rate 0.75 kg/s. Other boundary conditions were described in Table 3. The results of impeller designs modification are described in Table 6, Figure 10 and Figure 11. The main geometry sizes of compressor designs are presented on Table 4 and on Table 5.

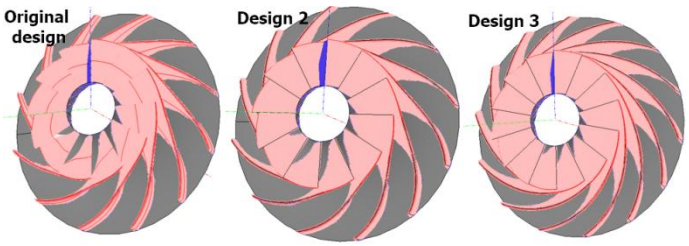

Figure 9: 3D view of impeller designs

Table 3. Geometry modifications for the impeller designs

	Original design	Design 2	Design 3
blade angle at out let, tan deg	36.5	27	27
Blade length, mm	36.37	37.38	41.84
Wrap angle, deg	-80	-80	-100.6
dβ/dm, rad/m	-25.52	-44.57	-28.03
Throat area, mm^2	427.82	485.86	444.06
number of blades	12	12	14
rotational speed, RPM	63000	65800	66800

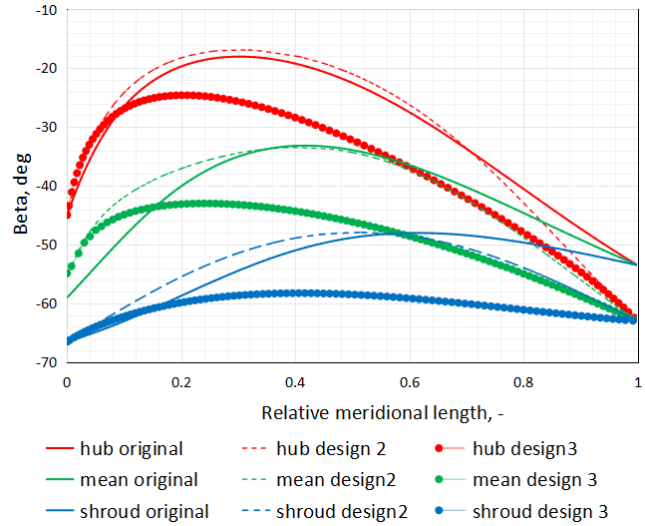

Figure 10: Blade angle distribution for the impeller designs (from meridional plane)

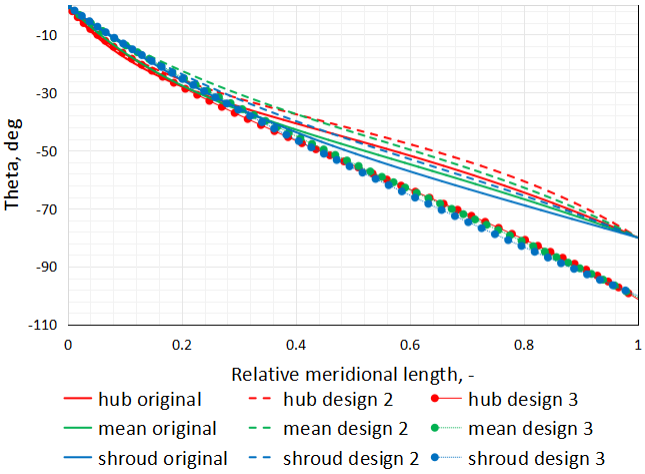

Figure 11: Wrap angle distribution for the impeller design

Table 4. The main geometry sizes for the impeller designs

	Original design	Design 2	Design 3
Impeller geometry			
Number of full blades	12	12	14
Hub inlet diameter	14 mm		
Shroud inlet diameter	37 mm		
Tip diameter, mm	58.5 mm		
Impeller Axial length	19 mm		
Leading edge blade thickness	0.35mm	0.35mm	0.34mm
Trailing edge blade thickness	0.3mm	0.3mm	0.32mm
Volute geometry			
inlet diameter, mm	87 mm		
outlet diameter, mm	106.36 mm		
equivalent outlet width, mm	15.73 mm		
equivalent outlet height	19.36 mm		
Inlet annulus area	857.9 mm^2		
Outlet annulus area	457 mm^2		

Table 51. Impeller blade profile definitions for the 3 impeller designs. Angles are in degrees.

	design 1		design 2		design 3	
Streamwise Relative Meridional Position	hub θ	shroud θ	hub θ	shroud θ	hub θ	shroud θ
0	0.00	0.00	0.00	0.00	0.00	0.00
0.1	-17.97	-13.91	-16.68	-13.20	-16.88	-13.48
0.2	-27.87	-25.64	-25.60	-23.66	-28.07	-25.19
0.3	-34.84	-35.42	-32.07	-32.35	-37.70	-36.00
0.4	-40.64	-43.66	-37.47	-39.85	-46.55	-46.22
0.5	-46.13	-50.78	-42.55	-46.60	-55.02	-55.98
0.6	-51.75	-57.18	-47.81	-52.95	-63.36	-65.37
0.7	-57.80	-63.13	-53.67	-59.18	-71.79	-74.44
0.8	-64.44	-68.84	-60.57	-65.57	-80.58	-83.24
0.9	-71.82	-74.44	-69.09	-72.40	-90.09	-91.76
1	-80.00	-80.00	-80.00	-80.00	-101.21	-100.00

A centrifugal compressor that was designed with the 2D code platform was analyzed to evaluate its characteristic behavior in Ansys CFX. Nine operating points for the original design were simulated in Ansys CFX for map generation. Maps from Ansys CFX were compared with maps from 2D code . 3D Ansys CFX had good agreement of the performance map trends and integral results to those from the 2D code map. There were some differences between the CFD and 2D performance maps, particularly near surge for design 2 and design 3. The point of special interest was the location of instability regarding stall and deep surge. Maps of total-to-total pressure ratio and total-to-total internal efficiency vs. mass flow rate are shown on Figure 12 and Figure 13, and on Figure 15 and Figure 16, respectively.

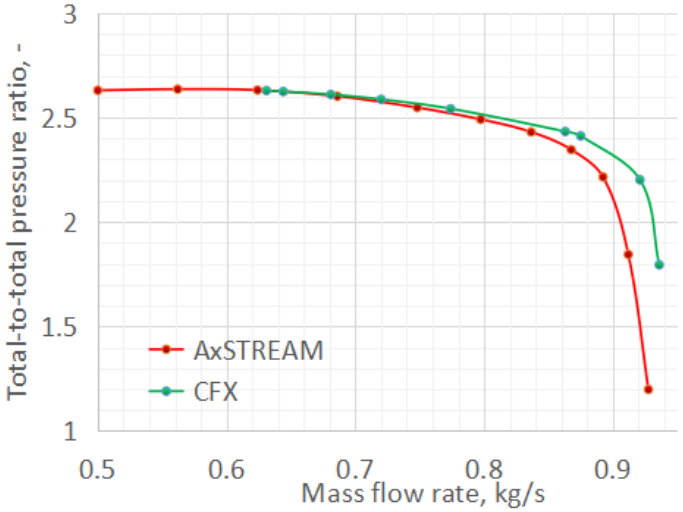

Figure 12: Operational map of compressor in coordinates "total-to-total pressure ratio vs. mass flow rate"

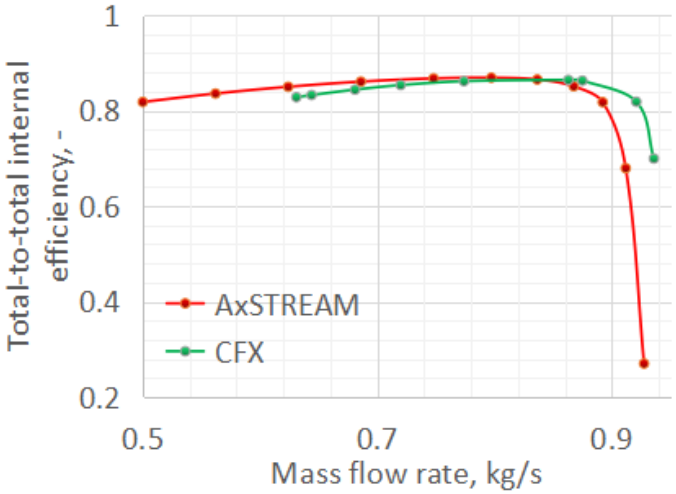

Figure 13: Operational map of compressor in coordinates "total-to-total internal efficiency vs. mass flow rate"

The streamline analysis shows stable flow in the compressor. An insignificant vortex region can be seen in volute diffuser (Figure 14).

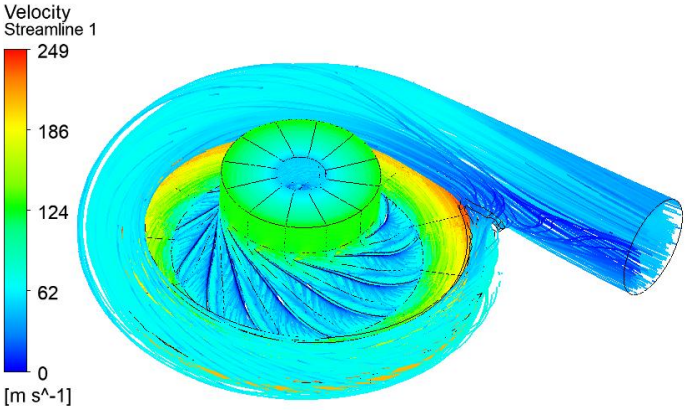

Figure 14: Streamline analysis for original design. Results in design point

In accordance with the main goal of the work, two additional compressor designs were with the aim to increase surge margin by means of increasing the pressure curve slope. Modeling details, requirements, and geometry difference for the impellers were described previously in section 2.2.

Five operational points for design 2 and ten operational points for design 3 were computed in Ansys CFX for the compressors maps (Figure 15, Figure 16).

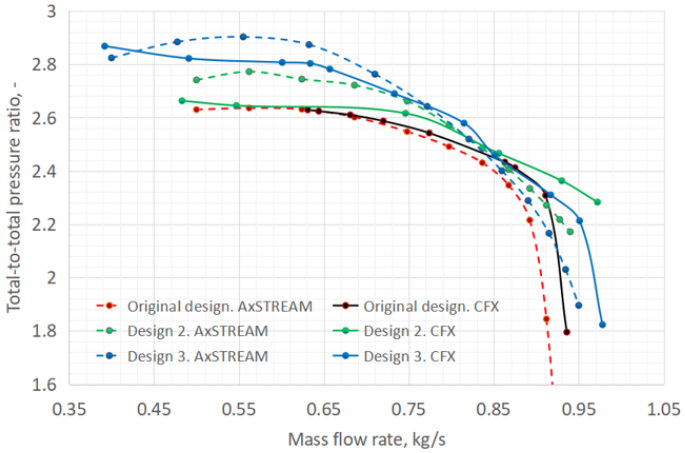

Figure 15: Operational maps of compressor in coordinates "total-to-total pressure ratio vs. mass flow rate". Comparison analysis for the original design, for the design 2 and for the design 3

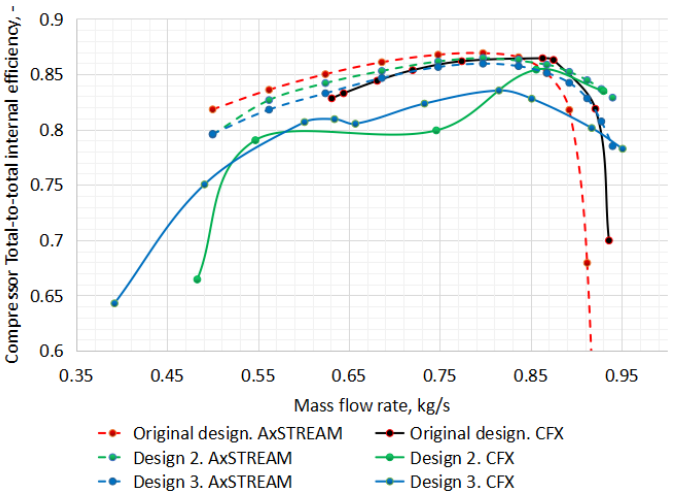

Figure 16: Operational maps of compressor in coordinates "total-to-total internal efficiency vs. mass flow rate". Comparison analysis for the original design, for the design 2 and for the design 3

3.1 Types of flow instability in a steady-state solution in CFD analysis

A type of flow instability in a steady-state solution was found during the CFD analysis: recirculation work at impeller inlet (in the near surge region). This effect has a major influence on the solution convergence and can increase numerical error of the solver.

The solver tries to converge to a steady solution of the flow field, but since surge is a transient phenomenon (there is no steady solution), the solver instead starts to oscillate at low mass flows, and it leads to questionable results for the left-most operating points (see results for the design 2 and the design 3 in Figure 16). The reason for the non-smooth operational map in CFX is the flow instability in steady-state analysis.

Recirculation work in the impeller can explain the flow instability effects in the steady-state analysis and the non-smooth trends of the performance maps from the 3D CFX analysis which are presented in Figure 15 and Figure 16.

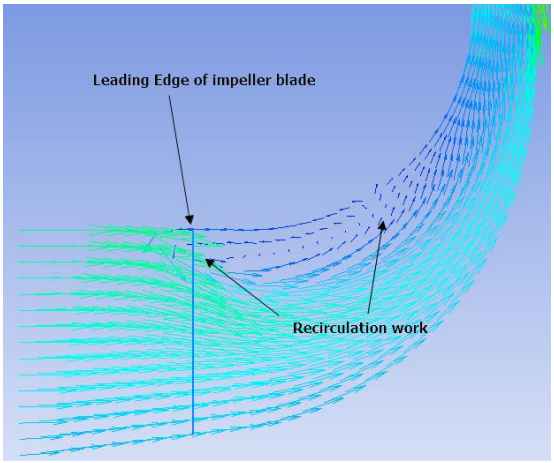

Figure 17: Velocity vectors analysis on meridional view for the design 2

To identify the recirculation phenomenon, the flow pattern in the impeller was analyzed in Ansys CFX for an operational point in the rotating stall region, and another at the design point for design 2. Velocity and temperature evaluations were taken from the surface which was aligned to the leading edge of the impeller. The meridional velocity is increased due to the aerodynamic blockage (Figure 18). The velocity triangles at the inlet increase their tangential component of absolute velocity. The increase of the tangential component to the absolute velocity is also evident and large enough to pay attention to this effect (Figure 19).

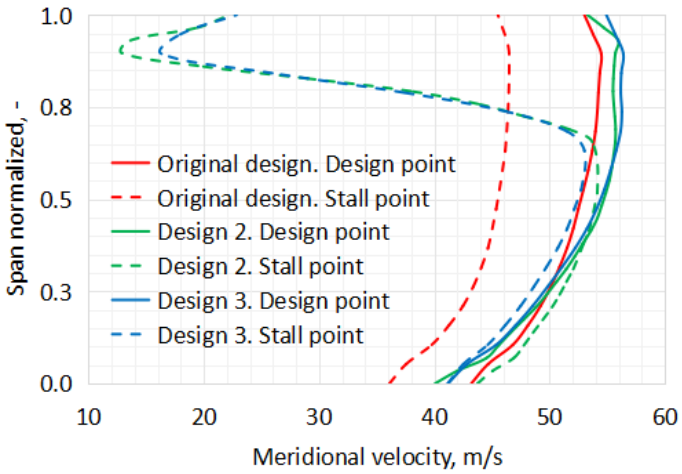

Figure 18: Meridional velocity distribution at impeller inlet for the design 2

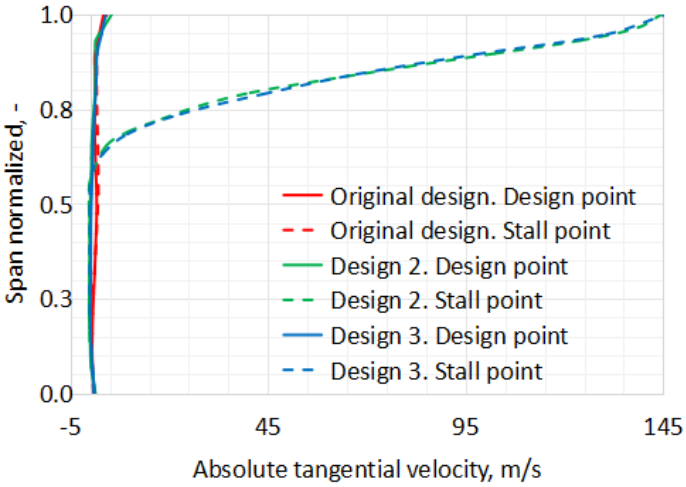

Figure 19: Absolute tangential velocity distribution at impeller inlet for the design 2

Also, the recirculation zone of the active flow results in an increase in total temperature. Due to the energy exchange in the region close to the shroud (in the recirculation zone), part of fluid being rejected back into the inlet domain causes the total temperature of the inlet flow to increase (Figure 20).

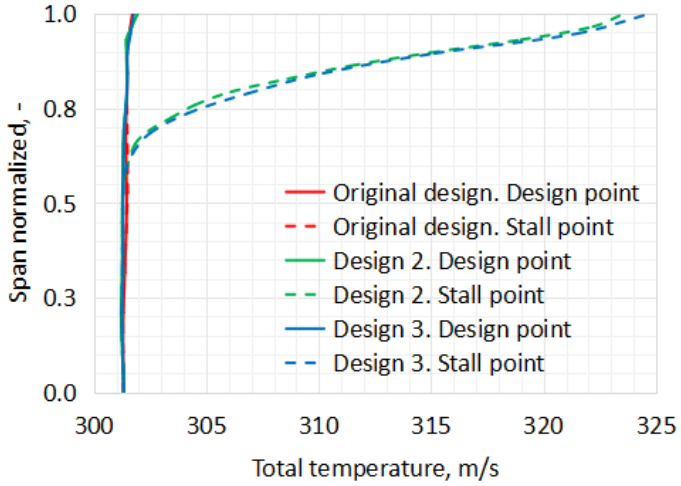

Figure 20: Total temperature distribution at impeller inlet for the design 2

3.2 The loss model tuning procedure in 2D code

A compressor was created in 2D code with tip clearance under a covered impeller with radial seals. The impeller in Ansys CFX was simulated without a shroud cavity system and without tip clearance. 2D code has a specified mass flow rate of the main flow and shrouded blade tip clearance leakage. Tip clearance leakage is a fluid leakage from the impeller discharge back to the inlet through the impeller eye seal and this is a type of parasitic work. Since the pressure rise imparted to this fluid is dissipated in the clearance gap and seal, the impeller works on this portion of the fluid twice, with no additional contribution to the pressure rise [23]. That is, the total mass flow rate in the impeller flow path is the sum of the main flow and flow through tip clearance leakage. For a correct comparison analysis between the 2D code and Ansys CFX, tip clearance was set to zero in 2D code and the working mass flow was taken as the sum of the main flow and flow through tip clearance leakage.

For example, for design 2 the total mass flow rate was equal to 0.8136 kg/s (mass flow rate in design point 0.75 kg/s and mass flow rate in tip clearance leakage 0.06357 kg/s). Maps for the 1D/2D method, which models the full flow path including secondary cavity, and CFD, which, although capable of modeling the full flow path is, for the purpose of simplifying the analysis only modeling the main impeller passage, cross over each other at the design point. To achieve intersection of the maps at the design point, loss models for the impeller can be calibrated in2D code.

The AxS RC dev Advanced deviation angle calculation model considers the derivative of blade angle along the meridian length at blade outlet. In this model, the deviation depends on the beta angle distribution at blade outlet. In general, the slip factor enables the determination of fluidic power difference between ideal and real impeller outflow conditions. For swirl-free inlet flow, the real circumferential outflow velocity is compared to an ideal circumferential velocity. In this case, the ideal outflow

velocity is the velocity conform to the impeller blade angle [15]. The compressor slip is a non-viscous and two-dimensional phenomenon. It can be explained with the relative channel vortex model. Due to the rotation of the impeller, the radial fluid flow is redirected in circumferential direction because of the centrifugal forces. This results in a speed and pressure gradient between the pressure and suction side. The gradient induces the relative channel vortex. The vortex causes a deflection of the fluid flow at the outlet [24]. Viscous and three-dimensional flow effects like the Coriolis vortex and other secondary flow phenomena reinforce this slip phenomenon. Furthermore, low kinetic energy fluid near the suction side changes the flow angle. Besides aerodynamic influences, the impeller geometry affects the secondary flow and thus the slip factor. The main two different slip factor definitions are known: the European and the American. The European definition of the slip factor is based on ideal circumferential velocity. In the American definition, the impeller tip speed at the outlet is used as the divisor. The advanced deviation model in 2D code uses the American definition of slip factor.

Since the difference in total-to-total pressure ratio at the real design point is insignificant, calibration of deviation angle model contains deviation angle scale only. The calibrated performance map in 2D code intersects with the map from Ansys CFX at the real design point mass flow rate (Figure 21).

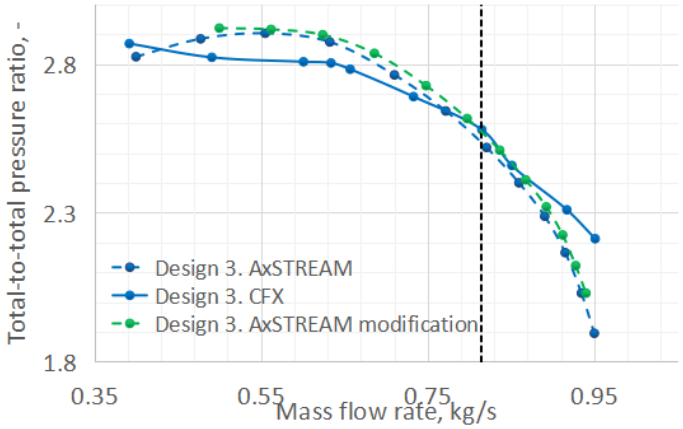

Figure 21: The real design point after loss models calibration determining for the design 3. Step 1

On the other hand, loss models for impellers can be calibrated with the Wiesner deviation angle model. As noted, before, there are two definitions of slip factor. Both are equal to one minus the normalized slip velocity. In one definition the amount of slip is normalized by dividing the slip velocity by the rotor rim speed and in the other by the ideal (without slip) circumferential fluid velocity component. The second one introduces the complication that the circumferential fluid velocity component is dependent on the flow through the impeller, except in the case of radial blades, when the two definitions are equivalent. The Wiesner model [21] uses the first definition:

$$\sigma_S = \frac{c_{2U}}{c_{2U\infty}} \tag{3}$$

As can be seen from Figure 21, in order to achieve the intersection between the 2D code map with map from the 3D CFX analysis, the deviation angle value was reduced by 21% compared to the value calculated from the Wiesner model. An important advantage of the Advanced deviation model compared to the Wiesner model is the consideration of the derivative of blade angle by meridian length at the blade outlet. Due to the numerical analysis of two deviation models in 2D code, the Advanced deviation angle model was preferred and more accurately predicted the impeller slip when compared with performance from 3D Ansys CFX. When loss model tuning was finished for each compressor design, operational maps were re-calculated with the required tip clearance. The total-to-total pressure ratio was found for each compressor design - 2.53 at the required mass flow rate value 0.75 kg/s. Maps with total-to-total pressure ratio are shown in Figure 22. Operational maps with total-to-total internal efficiency show a peak value (0.79%) at the design point for the design 3 (Figure 23). The efficiency value of design 3 is less than 1% lower than for the original design (0.80%).

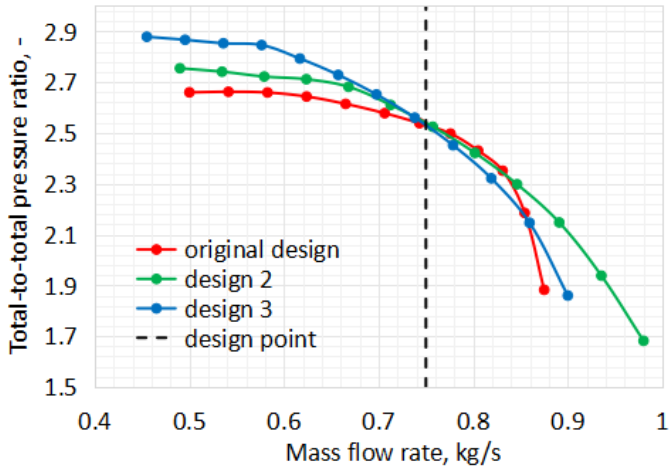

Figure 22: Operational maps of compressor in coordinates "total-to-total pressure ratio vs. mass flow rate" for the original design, for the design 2 and for the design 3 after loss model tuning

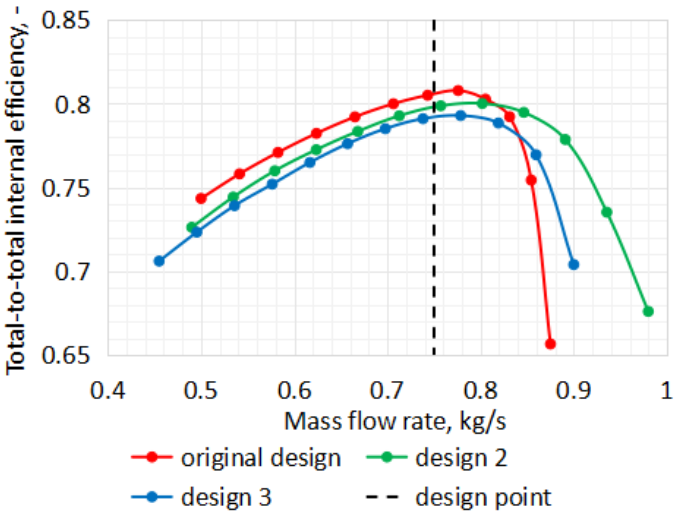

Figure 23: Operational maps of compressor in coordinates "total-to-total internal efficiency vs. mass flow rate" for the original design, for the design 2 and for the design 3 after loss model tuning

The blade loading distribution at the mean section for the original design, design 2 and design 3 is shown in Figure 24. The loading looks smooth, without significant peaks at the blade surfaces. The loading is reduced for design 3 compared to the other designs. We define blade loading as:

$$BL = 2\frac{P_p - P_s}{P_p + P_s}$$

Where P_p and P_s are the static pressure on the pressure and suction surfaces of the blade, respectively.

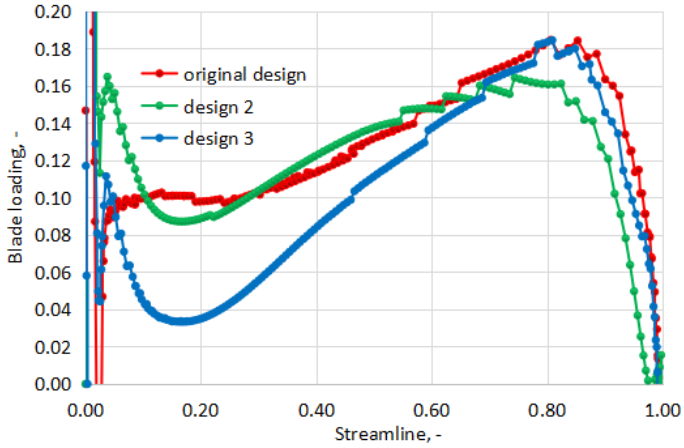

Figure 24: Blade loading for the original design, design 2 and design 3

The blade loading streamwise distribution reflects quite well the flow physics changes caused by the blade geometry modification. Design 2 was derived from design 1 by reducing the blade angle at outlet to achieve less blade loading on the blade tail due to higher relative velocity and to shift flow separation toward lower mass flow rates. Since the wrap angle was unchanged, the reduction of the blade angle resulted in the significant decrease of the blade angle derivative with respect to meridional length $d\beta/dm$ (Table 3). The green curve in Fig.24 shows this result, as the blade loading near the outlet of impeller design 2 is noticeably lower compared to design 1, while on the front part of blade it is the same because of the negligible geometry change near blade leading edge in design 2. Additionally, there is a sharp blade loading increase on the leading edge for design 2. This occurs due to the higher rotational speed for design 2 (Table 3), which results in a bigger incidence angle. Rotational speed was increased to compensate for the reduction of the outlet blade angle, while the inlet blade angle was unchanged at the same mass flow rate. Despite the bigger slope angle of the performance curve near the design point for design 2 (see Figure 15), the higher pressure at the stall operation mode was not achieved for design 2 compared to design 1 according to CFD results. This can be explained by the higher rotational speed, the bigger incidence loss in the impeller design 2 and, therefore, an earlier flow separation at the front part of impeller from leading edge to throat (more deed analysis was not performed in this work). Considering the shape of the performance curve obtained with 3D CFD (green solid curve in Figure 15) suggests that stall onset takes place somewhere between 0.7 and 0.75 kg/s. Design 3 was developed to crucially resolve the problem of increasing the stall margin. It inherited from design 2 the inlet and exit angles of the blade. To decrease the average blade loading, the number of blades increased from 12 to 14 and the wrap angle from 80 deg to 100 deg to increase blade length. The blade loading for design 3 at the design point is presented by a red curve in Figure 24. It can be noted that blade loading distribution near the trailing edge of design 3 is similar to that of the original design. This can be explained by the fact that wrap angle in design 3 was increased keeping the blade angles unchanged, resulting in the blade angle derivative $d\beta/dm$ increasing compared to design 2. This parameter in design 3 became close to that in design 1 (Table 3). This is why the blade loading near the trailing edge is similar for designs 1 and 3. But it is obvious that the average blade loading in design 3 is significantly lower compared to the other design variants. Moreover, increasing the wrap angle resulted in a smaller throat area compared to design 2 and reduced the blade channel expansion from leading edge to throat. This prevents the possible flow separation in front part of impeller that can be caused by positive incidence angle. Together with the lower average blade loading, this enabled shifting the stall onset toward smaller mass flow rates and increasing the outlet pressure at stall operation mode. On the performance curve obtained with 3D CFD for the design 3 (Figure 15) the stall inception can be defined at a mass flow rate 0.63 kg/s. A side effect from increasing the stability margin is the noticeable decrease of compressor efficiency, as seen in Figure 16. The larger number of blades and blade length increase in design 3 resulted in higher skin friction losses within blade channel. While the higher velocity level due to a larger rotational speed caused the higher overall losses in design 3. Tradeoff between peak efficiency and

stability margin is common occurrence during the development of a compressor flow path.

3.3 The Stall margin analysis

The research focus is to develop a centrifugal compressor with improved stall margin, as indicated by the lower flow rates at which the performance characteristic slope levels off. Methods for defining the stall margin were described before in section 2.3 Stall/Surge Analysis. Operational maps for the three compressor designs were computed in 2D analysis. The design point can be set as a working point and stall point defined from the operational maps.

An example of the stall margin definition which is based on 2D code operational maps is shown on Figure 25 for all compressor designs.

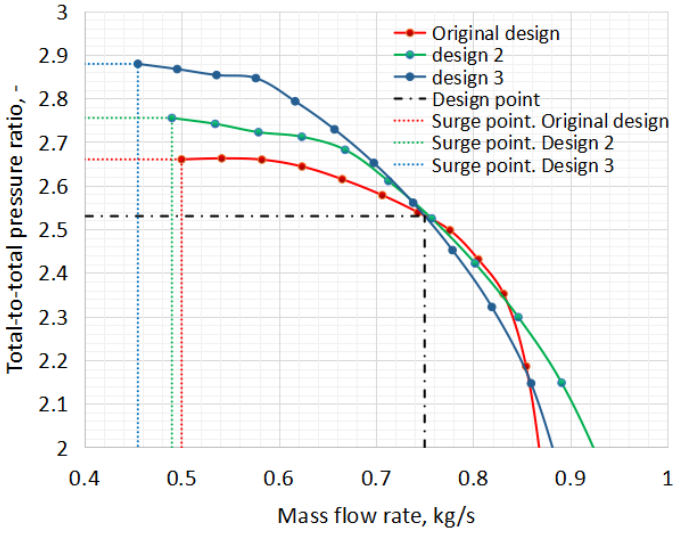

Figure 25: Surge margin definition by pressure slope for all compressor designs

Stall margins for each compressor design were calculated using two methods (Eq. (1), Eq. (2)). A performance comparison of the three compressor designs in 2D code is shown on Table 6.

Table 6. Comparison analysis of stall margin for each compressor design. Results are based on 2D code simulations

Parameters	Original design	Design 2	Design 3
ptr working	2.53	2.53	2.53
ptr stall	2.66	2.76	2.88
MFR working, kg/s	0.75	0.75	0.75
MFR stall, kg/s	0.50	0.49	0.46
Stall margin. Method 1	0.37	0.40	0.47
difference. Method 1, %	-	3.41	10.10
Stall margin in %. Method 2	5.14	8.90	13.80
difference. Method 2, %	-	3.75	8.66

Both stall margin methods (Method 1 and Method 2) show improvements across all designs, with the most significant improvements observed in design 3: 10% by Method 1 and 8.7% by Method 2. At the same time, the internal total-to-total efficiency value of design 3 is less than 1% lower than for the original design. Design 3 is the optimal tradeoff between a slight decrease in peak efficiency and significantly increased stability margin.

4. CONCLUSION

In this paper, research on the flow field and performance characteristics of a novel reference design centrifugal compressor for refrigerant compression was shown. Except for the goal of developing a compressor characteristic across an operating range, the main point of research is to characterize the surge margin and increase it by expanding the operational compressor range.

Three compressor designs for refrigerant compression have been presented in this paper. More specifically, a set of reference designs was developed for a compressor using R134a as the working fluid with boundary conditions corresponding to a typical heat pump application. The design used an integrally shrouded impeller wheel, which is often employed in process and refrigeration compression systems. Furthermore, several variants of the design were available to choose as baselines depending on high surge margin.

3D CFD analysis showed a flow instability effect in steady-state analysis of compressors. It has been noted that this phenomenon had major influence on the solution convergence and could increase numerical error for the CFD solver.

Compressor designs were created using 2D analysis with tip clearance under covered impeller with radial seals. CFD analysis considered only the main flow path without consideration of leakage flow through the secondary flow shroud cavity. Therefore, 2D code takes into account the sum of mass flow rate of the main flow and shrouded blade tip clearance leakage. Since the energy transferred to the leakage fluid is dissipated in the clearance gap and seal, the impeller works on this portion of the fluid twice, with no additional contribution to the pressure rise.

Analysis of the blade loading streamwise distribution using CFD simulation results reflected quite well the flow physics changes caused by the blade geometry modification. Average blade loading in design 3 is significantly lower compared to both previous variants. Together with the lower average blade loading this allowed shifting the stall onset toward smaller mass flow rate and increasing the outlet pressure at stall operation mode.

For correct comparison analysis between 2D code and CFD, tip clearance was set as zero value in 2D code and working mass flow was taken as the sum of the main flow and flow through from tip clearance leakage. Map comparisons between 2D code and CFD crossed each other in the real design point is the same for both tools. For achieving intersection of maps in design point, loss models were calibrated in the 2D code. Due to numerical analysis of two deviation model in 2D code (Wiesner and Advanced), Advanced deviation angle model predicts the impeller slip factor more accurately in wide range of the blade angle distribution and is more preferred to compare 1D and 2D

analysis with 3D CFD results. When loss models tuning was finished for each compressor design, operational maps were re-calculated with the required tip clearance. Total-to-total pressure ratio has been found for each compressor design - 2.53 with required mass flow rate value 0.75 kg/s. Maps with total-to-total pressure ratio are shown in Figure 22. Operational maps with total-to-total internal efficiency show peak value (79%) in design point for the design 3 (Figure 23). The efficiency value of design 3 is less than 1% lower than for the original design (80%).

Both surge margin methods (Method 1 and Method 2) show improvements across all designs, with the most significant improvements observed in design 3: 10% by Method 1 and 8.7% by Method 2.

Finally, it should be noted, as motivation for future research, that the research has potential application for simulation of transient CFD analysis, since a steady-state analysis determined the transient effects. Transient analyses were not within the scope of the present research, however, the potential to gain significant additional insight is recognized. Also, loss models in 2D code, such as secondary loss models, deviation angle loss models and blockage loss models can be modified based on results of CFD analysis. This work specifically perspective in this gap.

ACKNOWLEDGEMENTS

The authors would like to thank SoftInWay, Inc. for sponsoring this work and allowing its publication

REFERENCES

[1] Krain, H, Hoffmann, B, & Pak, H. "Aerodynamics of a Centrifugal Compressor Impeller With Transonic Inlet Conditions." Proceedings of the ASME 1995 International Gas Turbine and Aeroengine Congress and Exposition. Volume 1: Turbomachinery. Houston, Texas, USA. June 5–8, 1995. V001T01A011. ASME. https://doi.org/10.1115/95-GT-079

[2] Ziegler, K. U., Gallus , H. E., and Niehuis, R. (January 23, 2003). "A Study on Impeller-Diffuser Interaction—Part I: Influence on the Performance ." ASME. J. Turbomach. January 2003; 125(1): 173–182. https://doi.org/10.1115/1.1516814

[3] Ziegler, K. U., Gallus , H. E., and Niehuis, R. (January 23, 2003). "A Study on Impeller-Diffuser Interaction—Part II: Detailed Flow Analysis ." ASME. J. Turbomach. January 2003; 125(1): 183–192. https://doi.org/10.1115/1.1516815

[4] Medic, Gorazd, et al. High efficiency centrifugal compressor for rotorcraft applications. No. NASA/CR-2014-218114. National Aeronautics and Space Administration, 2014.

[5] Katz, Martin. Aktive Unterdrückung von Rotating Stall in einem Axialverdichter mit pulsierender Lufteinblasung. Diss. Technische Universität Darmstadt, 2002.

[6] Li, J., Wang, B., Zheng, X., Wang, Z., and Zheng, X. (March 11, 2024). "Experimental Investigation on the Aerodynamic Instability Process of a High-Speed Axial-Centrifugal Compressor." ASME. J. Eng. Gas Turbines Power. August 2024; 146(8): 081018. https://doi.org/10.1115/1.4064624

[7] Hu, J. Theory of Aviation Impeller; National Defense Industry Press: Beijing, China, 2014.

[8] Day, I. J. (October 13, 2015). "Stall, Surge, and 75 Years of Research." ASME. J. Turbomach. January 2016; 138(1): 011001. https://doi.org/10.1115/1.4031473

[9] Greitzer, E. M. (April 1, 1976). "Surge and Rotating Stall in Axial Flow Compressors—Part I: Theoretical Compression System Model." ASME. J. Eng. Power. April 1976; 98(2): 190–198. https://doi.org/10.1115/1.3446138

[10] Greitzer, E. M. (April 1, 1976). "Surge and Rotating Stall in Axial Flow Compressors—Part II: Experimental Results and Comparison With Theory." ASME. J. Eng. Power. April 1976; 98(2): 199–211. https://doi.org/10.1115/1.3446139

[11] Smith, J., & Zhang, H. (2019). "Impact of blade geometry on centrifugal compressor performance: A CFD study." Journal of Refrigeration Engineering, 35(4), 210-220.

[12] Brown, T., et al. (2020). "Investigating refrigerant flow and performance characteristics of centrifugal compressors under varying operational conditions." International Journal of Mechanical Engineering, 42(7), 1183-1198.

[13] Weiss, R., Bocker, B., & Sommer, S. (2021). "Comparative study of refrigerants R1234yf, R134a, and R452B in commercial refrigeration." International Journal of Refrigeration, 101, 77-88.

[14] Moroz, L., Govoruschenko, Y., Pagur, P., & Romanenko, L. (2008, January). Integrated conceptual design environment for centrifugal compressors flow path design. In *ASME International Mechanical Engineering Congress and Exposition* (Vol. 48753, pp. 175-185). https://doi.org/10.1115/IMECE2008-69122

[15] Aungier, Ronald H. "Centrifugal compressors." (2000): 187-194.

[16] Brunt, R., Liu, H., & Wang, Q. (2018). "Performance analysis of R1234yf, R452B, and R134a in various refrigeration systems." International Journal of Refrigeration, 89, 123-134

[17] Tillner-Roth, R. and Baehr, H.D., "An international standard formulation of the thermodynamic properties of 1,1,1,2-tetrafluoroethane (HFC-134a) for temperatures from 170 K to 455 K at pressures up to 70 MPa," J. Phys. Chem. Ref. Data, 23:657-729, 1994.

[18] Goldenberg, V, Conser, B, & Vorobyova, A. "A Method of Pseudo-Steady State CFD Calculation to Predict Turbomachine Characteristics." Proceedings of the ASME Turbo Expo 2023: Turbomachinery Technical Conference and Exposition. Volume 13C: Turbomachinery — Deposition, Erosion, Fouling, and Icing; Design Methods and CFD Modeling for Turbomachinery; Ducts, Noise, and Component Interactions. Boston, Massachusetts, USA. June 26–30, 2023. V13CT32A005. ASME. https://doi.org/10.1115/GT2023-101016

[19] Li, J.; Wang, B.; Zheng, X. Surge Process of a High-Speed Axial–Centrifugal Compressor. Processes 2023, 11, 2869. https://doi.org/10.3390/pr11102869

[20] Eckert, B. & Schnell, E. & Kestin, J. (1962). Axial und Radial Kompressoren. Journal of Applied Mechanics. 29. 10.1115/1.3636480.
[21] Tubbs, H. "Compressor Aerodynamics. By NA CUMPSTY. Longman, 1989. 509 pp.£ 49." Journal of Fluid Mechanics 226 (1991): 659-659.
[22] Van den Braembussche, Rene. Design and analysis of centrifugal compressors. John Wiley & Sons, 2018.
[23] Waesker, Markus, et al. "Analysis of slip factors in CFD calculations–Assessment of literature models." 14 th European Conference on Turbomachinery Fluid dynamics & Thermodynamics. EUROPEAN TURBOMACHINERY SOCIETY, 2021.https://doi.org/10.29008/ETC2021-528
[24] von Backström, T. W. (August 10, 2005). "A Unified Correlation for Slip Factor in Centrifugal Impellers." ASME. J. Turbomach. January 2006; 128(1): 1–10. https://doi.org/10.1115/1.2101853